

Noise Spectroscopy of Transport and Ion-Related Phenomena in Silicon Nanowire Field-Effect Transistor Biosensors

Yangyan Guo, Denys Pustovyi, Yurii Kutovyi, Nazarii Boichuk, Mykhailo Petrychuk, Yongqiang Zhang, and Svetlana Vitusevich*

High-quality, liquid-gated two-layer (TL) nanowire (NW) field-effect transistor (FET) structures are fabricated and studied in different operation regimes and with different concentrations of MgCl_2 solutions. The space-charge-limited current (SCLC) effect is sensitive to surface phenomena and is registered at the drain-source voltage (V_{DS}) above 0.14 V, and analyzed using several methods including noise spectroscopy. Noise spectra reflect the clear transformation from $1/f$ to $1/(f \text{ in power } 1.5)$ behavior, confirming the SCLC effect, which is sensitive to ion processes at the NW FET surface. Moreover, the dimensionless Hooge parameters, measured at a level of 10^{-3} , reflect the high quality of the fabricated devices and demonstrate the suppression of noise with V_{DS} increasing up to 0.48 V. Such behavior additionally confirms the SCLC effect in the NW channel. The effect of suppression is stronger for small concentrations of MgCl_2 solutions. The results should be taken into account for the detection of very small signals in biochemical solutions.

sensing principle of FETs is the adsorption of charged analytes on the sensor surface, which results in a change of electrical potential to induce a detectable signal in the form of current change. A new approach for enhanced sensitivity is suggested based on the single trap phenomena^[2] and demonstrated in nanowire devices with a liquid gate filled with different biochemical liquids including phosphate buffered saline (PBS). The actual biochemical detection is often in a solution system where the solid-liquid interface responds to the complex multi-ion environment. To expand the sensor applications and verify signal reliability, it is essential to study the effect of ion concentrations in biochemical solutions on the sensor-solution interface, especially for small analyte concentrations.

1. Introduction

Nanoelectronic biosensing technology has developed significantly in recent decades. A variety of biosensors based on field-effect transistor (FET) device platforms have been suggested and applied in biochemical sensing applications.^[1] The basic


To study the composition of the ion effect at the sensor-solution interface and the electrical signal response of the device to different ions is of great significance for the expansion of the sensor detection principles and the verification of signal registration reliability, especially for small concentrations of biochemical solutions.

Nanostructures have already been confirmed to be an ultra-sensitive platform to study the monovalent ion system (e.g. KCl and NaCl) and the divalent ion system in nanofluidic ionic transport.^[3] Charge inversion phenomena can be observed during the sensing measurement, which means that more counterions can be found inside the electric double layer than are needed to compensate for the surface charge. Though this phenomenon was reported a century ago, recent research suggests that the ion-ion correlation is the likely origin of charge inversion.^[4] The site-binding mode (SBM) mechanism^[5] of inorganic salt ions on the oxide surface was previously reported.^[6] The semiempirical Nikolsky theory is also used to estimate the selectivity of sensors against interfering ions.^[7]

The FET sensing ability typically requires the assistance of a given surface coating to promote the selectivity of ion sensing.^[8] Sivakumarasamy^[9] et al. developed a silicon nanotransistor with sizes scaled down to ≈ 25 nm to exploit ion-specific surface interaction without requiring a selective organic layer. They tested this method with blood serum containing Na^+ , K^+ , Ca^{2+} , and Mg^{2+} . A lack of understanding of ion-surface interaction on pure solid semiconductor materials gives rise to many inconsistencies in the same sensors for different biochemical sensing systems.

Y. Guo, D. Pustovyi, Y. Kutovyi, N. Boichuk, Y. Zhang, S. Vitusevich
Institute of Biological Information Processing (IBI-3)
Forschungszentrum Jülich
52425 Jülich, Germany
E-mail: s.vitusevich@fz-juelich.de

Y. Guo
On leave from the Institute of Semiconductors
Chinese Academy of Science
Beijing 100083, China
M. Petrychuk
Faculty of Radiophysics
Electronics and Computer Systems
Taras Shevchenko National University of Kyiv
Kyiv 03127, Ukraine

 The ORCID identification number(s) for the author(s) of this article can be found under <https://doi.org/10.1002/admi.202201142>.

© 2022 The Authors. Advanced Materials Interfaces published by Wiley-VCH GmbH. This is an open access article under the terms of the Creative Commons Attribution-NonCommercial-NoDerivs License, which permits use and distribution in any medium, provided the original work is properly cited, the use is non-commercial and no modifications or adaptations are made.

DOI: 10.1002/admi.202201142

Kobab et al. studied the buffer capacity effect of electrolyte solutions on ion sensitive FET (ISFET) sensitivity, and found that by increasing a certain counterion size, ISFET sensitivity can be greatly enhanced.^[10] Therefore, the charge formed at the nanowire surface can be effectively used to influence biosensor transport phenomena and to improve the detection limit of such devices. The space-charge-limited current (SCLC) effect^[11] is known to be very sensitive to trapping processes on the surface of solids. Several reports confirmed the importance of the SCLC effect for carrier redistribution studies in nanowire structures of GaN, InAs, CdS, GaAs, and ZnO.^[12] However, the SCLC effect in liquid-gated nanowire FET sensors has not been addressed in the literature.

In this work, we developed single silicon nanowire (NW) FETs with a SiO₂ layer to study the Mg²⁺ ion sensing process in a range from 10⁻⁶ to 10⁻¹ M. It should be noted that MgCl₂ solutions play an important role in many enzymatic reactions, DNA folding, and its concentration in human body solutions: blood, serum, saliva may reflect gastrointestinal disorder the disease or syndrome.^[13] We registered superlinear behavior in *I*-*V* characteristics with a characteristic power equal to 2 due to the SCLC effect after the linear transport regime. The SCLC regime is very sensitive to the ion processes on the surface of NW FETs. Moreover, we used noise spectroscopy to study the contribution of surface properties determined by ions on the nanowire surface and resulting fluctuation phenomena with a characteristic power (1.5) noise spectra. Such behavior is characteristic of diffusion noise and is in good agreement with the transport mechanisms in nanowire FET sensors.

2. Results and Discussion

Silicon NW FET structures with a liquid gate (LG) are ultra-sensitive key devices for biochemical studies. In this work, we study the transport and noise properties of unique two-layer (TL) LG NW FET devices with different concentrations of MgCl₂ solutions in a wide range of LG voltages, *V*_{LG}, and drain-source voltages, *V*_{DS}, using the *I*-*V* characterization technique, and noise spectroscopy. TL NW FET structures have several advantages, including the additional doping layer improves the device stability when working in direct contact with liquids,^[2]

moreover, the higher the doping, the smaller the influence of impurities introduced by the liquid environment, as was shown in single doped structures.^[14] Also, an almost undoped silicon layer followed by an additional doping layer^[2] is preferential to reach desired low level of noise in silicon-based nanostructures. This is important for liquid-gated sensors device structures, where the level of useful signal from molecules is usually very small. In addition, the noise level can be considerably reduced in the case of operation of the structure in the SCLC regime, as is shown below.

Current-voltage (*I*-*V*) characteristics of TL LG NW FET structures are studied in different concentrations of MgCl₂ solutions ranging from 10⁻⁶ to 10⁻¹ M. Several nanowire transistors were studied with widths, *W*, ranging from 150 to 90 nm and lengths, *L*, ranging from 200 to 2000 nm. The TL channel is formed by epitaxial growth of a 25 nm moderately doped (10¹⁶ cm⁻³) layer on 50 nm of low-doped (10¹⁵ cm⁻³) silicon on insulator wafer (SOI). Schematic representation of the structure is shown in the left inset in Figure 1A. All NW devices demonstrate similar behavior. Typical *I*-*V* characteristics measured for liquid-gated NW FETs of channel width *W* = 100 nm and *L* = 800 nm are shown in Figure 1A. The transfer characteristics of the drain current as a function of liquid-gate voltage *I*_D(*V*_{LG}) demonstrate behavior usually observed for field-effect transistors and good control of current in the channel with applied liquid-gate voltage. As the concentration of MgCl₂ increases, the current decreases due to the charge introduced by the Mg²⁺ ions attached to the nanowire sensor. Mg²⁺ ion-sensitive devices show a threshold voltage change of about 44 mV/decade molar ion concentration (Figure 1B).

Current-voltage output characteristics *I*_D(*V*_{DS}) are linear up to a voltage of *V*_{DS} = 0.14 – 0.25 V. However, at certain voltages (above 0.14 V), they demonstrate behavior approaching quadratic dependence (Figure 2). To demonstrate the transformation region to the quadratic dependence most clearly, we calculated the differential conductances and plotted their value as a function of drain-source voltage applied to the channel (Figure 2C). Section *G*_{diff} = Const (horizontal dashed line) corresponds to the linear dependence: *I*_{DS} ~ *V*_{DS}. Section with the linear dependence of *G*_{diff}(*V*_{DS}) corresponds to the quadratic dependence: *I*_D ~ *V*_{DS}². The characteristic voltage at which linear behavior changes to quadratic one is increased with change of

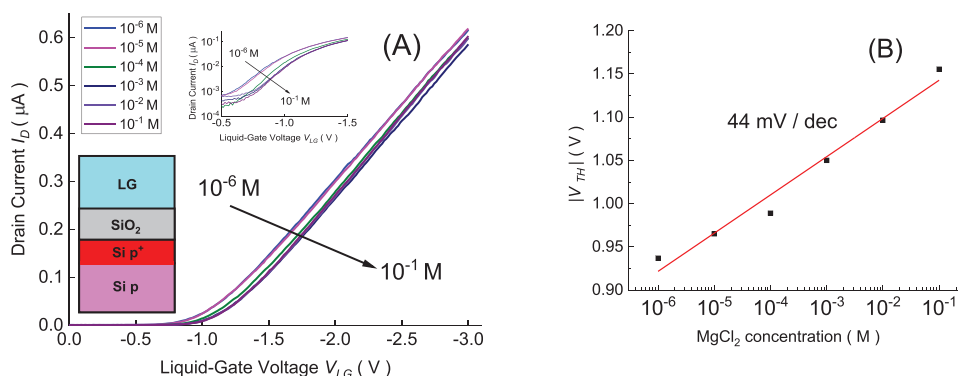


Figure 1. A) Typical transfer characteristics of *I*_D(*V*_{LG}), measured for a liquid-gated two-layer (TL) nanowire (NW) field-effect transistor (FET) with *W* = 100 nm and *L* = 800 nm at *V*_{DS} = 100 mV in six MgCl₂ solutions ranging from 10⁻⁶ to 10⁻¹ M. The right inset shows *I*-*V* characteristics in semi logarithmic scale, the left inset left shows schematic presentation of two-layer nanowire structure, where red color corresponds to *p*⁺-type of 10¹⁶ cm⁻³ doping, pink color corresponding to *p*-type of 10¹⁵ cm⁻³ doping. B) Extracted threshold voltage, *V*_{th}, dependence as a function of the concentration of MgCl₂ solutions.

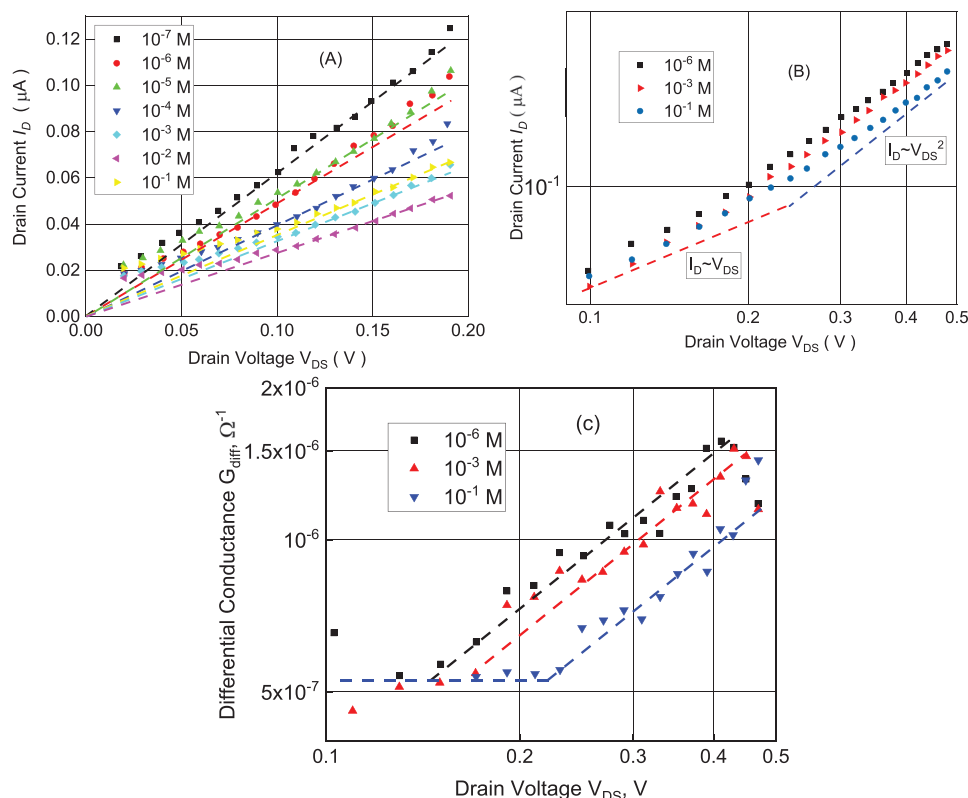


Figure 2. Output characteristics $I_D(V_{DS})$ of a liquid-gated two-layer (TL) nanowire (NW) field-effect transistor (FET) sensor with $W = 100$ nm and $L = 800$ nm, measured at $V_{LG} = -1.2$ V. A) The dashed lines show the corresponding linear dependencies obtained at voltages below 0.2 V, which changes to B) quadratic behavior at voltages above 0.14 V, shown in double logarithmic scale. C) The differential conductance dependence on drain-source voltage, $G_{diff}(V_{DS})$, obtained for different $MgCl_2$ solutions, shown in double logarithmic scale. The characteristic voltage at which linear behavior changes to quadratic one is equal to 0.145, 0.165, and 0.220 V for 10^{-6} , 10^{-3} , 10^{-1} M solution concentration, respectively.

concentration of $MgCl_2$ solution and is equal to 0.145, 0.165, and 0.220 V for 10^{-6} , 10^{-3} , and 10^{-1} M concentration, respectively.

Such behavior is characteristic of the SCLC effect in the nanowire channel.^[12,15] Moreover noise spectra show features confirming SCLC regime formation as shown below. SCLC is characterized by its super linear dependence on the applied voltage V_{DS} independent of the width of the sample, in accordance with the Mott–Gurney law:^[16]

$$I_D = \zeta \frac{\epsilon \mu V_{DS}^2}{4\pi L} \quad (1)$$

where ζ is a coefficient of the order of unity, ϵ is the permittivity, μ is the mobility of free current carriers, and L is the length of the nanowire.

In this case, at a definite V_{DS} , transport in the channel starts to exceed the ohmic current behavior due to the contribution of the surface states of a nanowire with a small width. The distribution of free carriers in the channel is strongly regulated by the adsorption of ions on the surface of p-type-doped NW FET sensors. Holes injected from an implanted region of the source (heavily doped by boron) to the nanowire FET determine the transport properties in the NW channel. SCLC studies reflect the density of the trap states and their energy depth.^[13] Thus, the SCLC effect provides important information about the charge transfer mechanisms in NW FET sensors. The attach-

ment of ions to the surface of the NW FET device results in the modification of the carrier profile inside the NW channel. Ions on the NW surface significantly influence the carrier transport and the noise properties of NW FET sensors as a result of the large surface-to-volume ratio of the NW channel.

It should be noted, that previously we studied NW FET samples in 10×10^{-3} M PBS solutions,^[2] where the main salt was 140×10^{-3} M NaCl in the solution.^[17] In this case single Na^+ ions compete with counterions at the solid–liquid interface. In the present work, $MgCl_2$ solutions contain divalent charged Mg^{2+} ions, which make a stronger contribution to the change of surface charge density at the solid–liquid interface than Na^+ ions. In the case of NW FET structures operating with $MgCl_2$ solutions, we registered and studied the SCLC effect using I – V characteristics and noise spectroscopy. The transport properties of NW FET sensors are determined by the density of surface states and NW doping levels.^[18] The voltage at which the conductivity transforms from ohmic to SCLC behavior reflects the transition region corresponding to transport where the injected carriers from a contact exceed the free carriers in the channel, which responds more effectively to surface states. Noise spectroscopy is known to be a powerful method to study the performance of nanodevice structures and their transport properties.^[15,19] We therefore applied noise spectroscopy to obtain detailed information about the ion processes taking place in the liquid-gated nanowire sensors.

3. Noise Spectroscopy of Liquid-Gated NW FET Sensors

The noise spectra of the samples were measured in the frequency range of 1 Hz–10 kHz. Noise spectra follow the law $1/f^\gamma$, where $\gamma \geq 1$ with some small deviation from this law. To determine the fine structure, the voltage noise spectra $S_v(f)$ are replotted to obtain the frequency dependencies of the dimensionless Hooke parameter $\alpha_H(f)$.^[20]

$$\alpha_H(f) = \frac{S_i(f)}{V_{DS}^2} \frac{fL^2R}{q\mu_p} \quad (2)$$

Here, α_H is the dimensionless Hooke parameter characterizing the noise level of the sample being tested; μ_p is the major carrier mobility; L is the sample length; R is the resistance of the sample; S_i is the current noise spectral density; and q is the elementary charge.

With these coordinates, the $1/f$ spectrum is transformed into a horizontal line, and deviations from the $1/f$ form become more accessible for analysis. This representation was chosen because in this case, the spectra are normalized over all parameters and the α_H parameter is dimensionless. The obtained spectra plotted in such coordinates reveal the features associated with the state of the electrolyte ions at the interface with the SiO₂ dielectric layer. About 100 spectra were measured to present the average behavior in a smoothed form. See more detailed information in the “Statistical Analysis” section below. Typical noise spectra are shown in Figure 3. All spectra feature at least two frequency regions: the first with a unit slope ($\gamma = 1$), the second region with $\gamma = 1.5$. Several features of interest can be identified and the spectra as a whole can be described as follows. For all concentrations of MgCl₂ solutions, there is a low-frequency component of the spectrum $1/f^\gamma$ where $\gamma = 1$, which changes to $\gamma = 1.5$ with increasing frequency. In different operation regimes of the NW sensor (V_{DS} , V_{LG}), even two slopes can be resolved in the

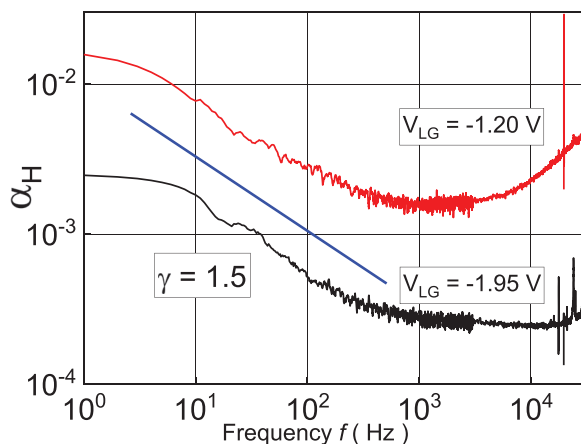


Figure 3. Typical noise spectra $\alpha_H(f)$ obtained for a liquid-gated two-layer (TL) nanowire (NW) field-effect transistor (FET) sensor with $W = 100$ nm and $L = 800$ nm in two operation regimes: near the threshold ($V_{LG} = -1.2$ V) and well above the threshold ($V_{LG} = -1.95$ V) demonstrating characteristic slope 1.5 for 10^{-5} M MgCl₂ liquid solution.

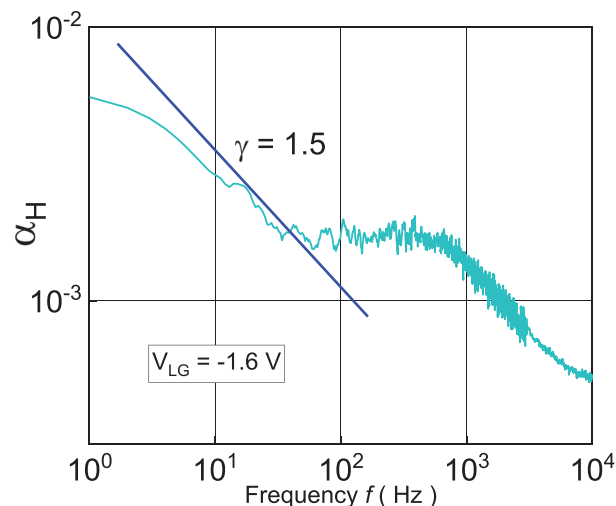


Figure 4. Noise spectrum $\alpha_H(f)$ obtained for a liquid-gated two-layer (TL) nanowire (NW) field-effect transistor (FET) sensor with $W = 100$ nm and $L = 800$ nm demonstrating the formation of two steps in 10^{-4} M MgCl₂ solutions.

noise spectra. However, the characteristic features described above reflect a common behavior in the device structures. Typical spectra are shown below in Figure 3.

The transition frequency of $\gamma = 1$ –1.5 varies within a range of ≈ 1 –10 Hz for all measured sensors. The most interesting feature in the noise spectra is the registration of not only the first step with a slope of 1.5, but of an additional region with a slope of 1.5 after the horizontal transition region with the characteristic slope described above in the high-frequency region of the spectra. In this case, two “steps” are clearly observed. Typical spectra with two steps are shown in Figure 4. The second step may have a transition frequency at another frequency (see Figure 5).

Moreover, at a very low concentration of MgCl₂, a Lorentzian-type spectrum (see Figure 6) can be registered instead of the first and/or the second step. The frequencies at which the

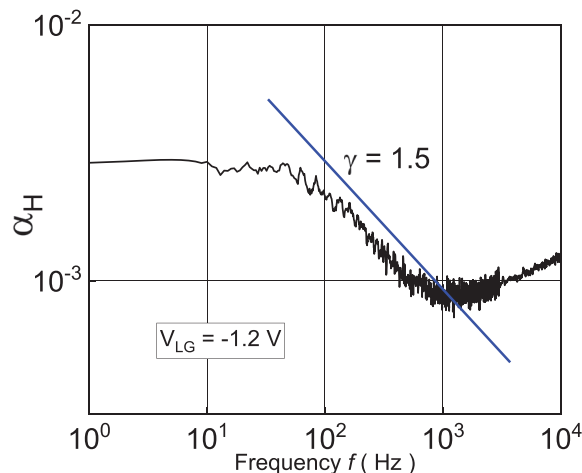


Figure 5. Noise spectrum $\alpha_H(f)$ obtained for a liquid-gated two-layer (TL) nanowire (NW) field-effect transistor (FET) sensor with $W = 100$ nm and $L = 800$ nm for the case of high-frequency step dominance in a 10^{-5} M MgCl₂ liquid solution.

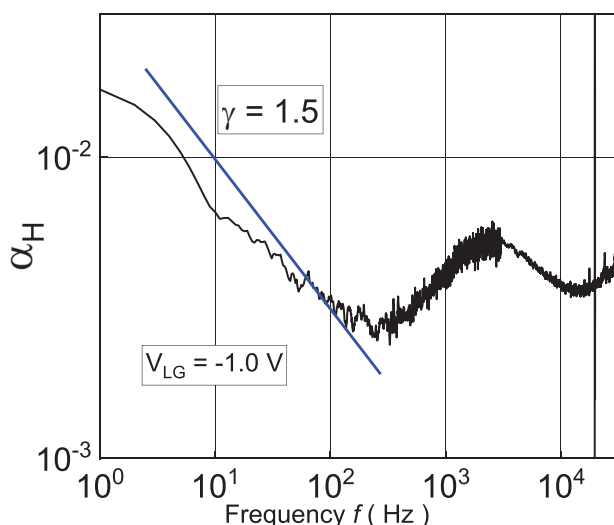


Figure 6. Noise spectrum $\alpha_H(f)$ obtained for a liquid-gated two-layer (TL) nanowire (NW) field-effect transistor (FET) sensor with $W = 100$ nm and $L = 800$ nm demonstrating a well-resolved Lorentzian component in a 10^{-6} M MgCl_2 solution.

Lorentzians are observed coincide with the frequencies of transitions of the spectrum curves from $\gamma = 1 - 1.5$.

The behavior of the noise spectra described above is similar to that of the nonequilibrium noise spectra in AlGaIn/GaN gateless structures measured without liquids.^[15] The spectra with characteristic behavior corresponding to the SCLC effect arise due to the strong electrostatic coupling of mobile carrier charges in the channel with weakly mobile charges on the surface. However, the conditions are different in the liquid-gated structures studied here, in which electrolyte ions play the role of weakly mobile charges. The registered transformation of noise spectra from $1/f$ to $1/f^{1.5}$ confirms the SCLC effect. For the case of SCLC free carrier concentration and their part that is captured on surface states are in the nonequilibrium state.^[12a,16,21] At large drain-source voltages, nonuniformly distributed noise sources due to ions on the surface result in diffusion processes

with a characteristic (1.5) slope in $1/f^{1.5}$ behavior.^[19] The frequency of the transition from $\gamma = 1$ to 1.5 in this case depends on the ion mobility, i.e. the nature and state of the ions near the Si/SiO₂ interface. Thus, it becomes possible to study the characteristics of the transition layer due to the ion processes near the gate insulator of the LG TL NW FET structure. At the silica surface, SiO⁻ charges are screened by Mg²⁺ counterions in the Stern layer.^[8] Other ions lead to an overscreening effect due to interaction with silanol groups via non-Coulombic hydrophilic forces causing a hydration effect within the Stern layer. The presence of two or more steps in this case may indicate the presence of two or more populations of ions with different properties that determine their mobility. The noise level reflects processes related to ions moving on the surface of the LG TL NW FET and corresponds to the mobility of ions on the channel surface.

It should be noted that the conditions for the electrostatic interaction between the main and surface conduction channels in the structures studied differ from the conditions in AlGaIn/GaN structures. In our liquid-gated structures, ion drift occurs predominantly as a result of a change in the surface charge influencing the charge of the main channel. The presence of Lorentzians in the noise spectra can be explained by recombination of injected carriers in the SCLC region^[15] and a diffusion noise component sensitive to the electrolyte charge due to electrostatic coupling between two parallel channels: silicon and surface ionic channels. Dimensionless Hooft parameters estimated for different drain-source voltages, also corresponding to the SCLC regime, are on the order of 10^{-3} , reflecting the good quality of liquid-gated NW FET structures. Families of frequency dependencies of Hooft parameters obtained for two electrolyte concentrations: 10^{-5} M (Figure 7A) and 10^{-1} M (Figure 7B) are shown below.

The important noise behavior should be particularly emphasized. The level of noise, i.e. the value of α_H , decreases monotonically with an increase in V_{DS} . In the case of low electrolyte concentrations, this drop is twice as large as the drop in the case of high concentrations. This additionally confirms the contribution of the SCLC effect to the formation of transport

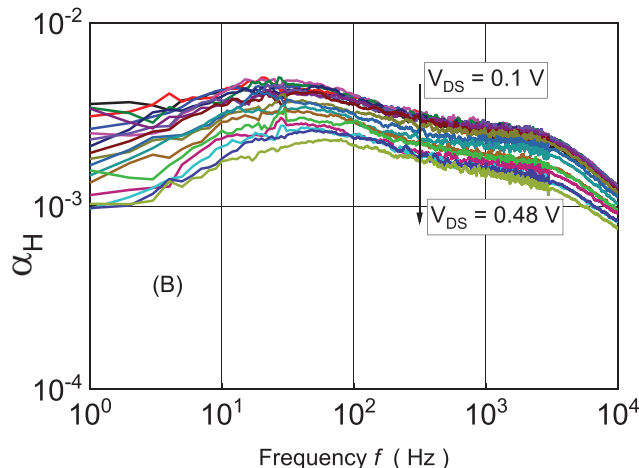
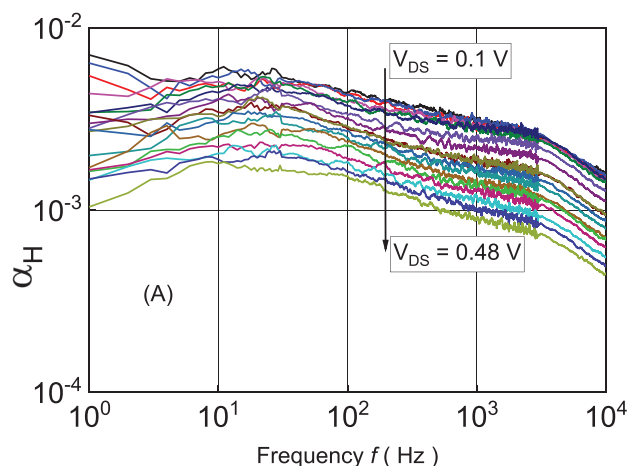


Figure 7. Frequency dependence of Hooft parameter $\alpha_H(f)$ obtained for a liquid-gated two-layer (TL) nanowire (NW) field-effect transistor (FET) sensor with $W = 100$ nm and $L = 800$ nm at $V_{LG} = -1.2$ V and drain-source voltages, V_{DS} , ranging from $V_{DS} = 0.10$ to 0.48 V in MgCl_2 solutions with concentrations of A) 10^{-5} M and B) 10^{-1} M.

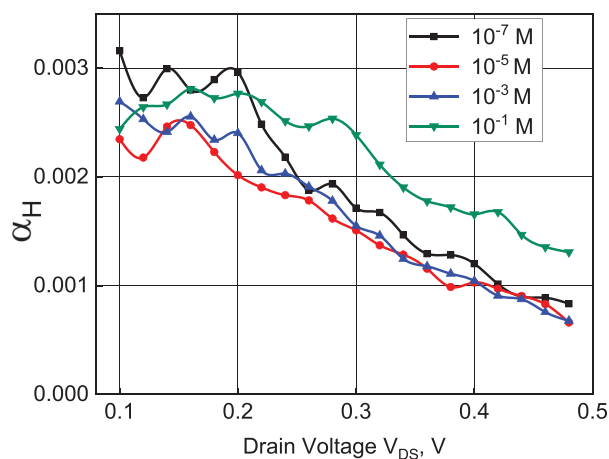


Figure 8. Hooe parameter α_H as a function of drain voltage, V_{DS} , obtained for a liquid-gated two-layer (TL) nanowire (NW) field-effect transistor (FET) sensor with $W = 100$ nm and $L = 800$ nm at $V_{LG} = -1.2$ V and frequency $f = 1$ kHz in $MgCl_2$ solutions with different concentrations from 10^{-6} to 10^{-1} M.

in LG TL NW FET devices. Several slopes can be registered in the noise spectra. In addition, a number of local maxima are observed in α_H vs. V_{DS} dependencies (Figure 8). Such behavior is characteristic of the SCLC effect.^[15] The fact also confirms the nature of the transport phenomenon in the nanowire channel corresponds to the SCLC regime.

It should be emphasized that the advantages of the SCLC effect in LG TL NW FET sensors operating in $MgCl_2$ solutions are increased sensitivity and reduced noise level. The increased sensitivity is due to the increase in I - V slope to a quadratic behavior at large drain-source voltages. At $V_{DS} = 0.48$ V, this nearly triple the sensitivity compared to the linear region at $V_{DS} < 0.2$ V (Figure 2C). The reduced noise level (shown in Figures 7 and 8) is due to SCLC regime. Together these effects represent strong potential of improving the signal-to-noise ratio of NW FET sensors.

4. Conclusions

Transport and noise properties of fabricated liquid-gated TL NW FET sensors were investigated in a wide range of voltages and concentrations of $MgCl_2$ solutions. Noise spectra demonstrate a clear transition from flicker noise to $1/f^{1.5}$ behavior, reflecting processes on the surface of NW FET sensors with characteristics of diffusion transport. The SCLC effect is revealed and confirmed by the suppression of Hooe parameters with increasing V_{DS} up to 0.48 V. The suppression effect is stronger for small concentrations of ions in solution compared to larger concentrations. These results open perspectives to increase signal-to-noise-ratio in NW FET sensors.

5. Experimental Section

The devices being studied are the unique two-layer liquid-gated silicon nanowire FET sensors fabricated using CMOS-compatible technology.

The fabrication started from $\langle 100 \rangle$ -oriented SOI wafers, in which the thickness of the buried oxide layer was 145 nm and the thickness of the top silicon layer was 50 nm. The top silicon layer was low p-type doped and the doping concentration was 10^{15} cm^{-3} . Based on the top silicon layer, a roughly 25 nm moderate doped silicon layer is first epitaxially grown using chemical vapor deposition. This new silicon layer was moderate boron-doped with a concentration of 10^{16} cm^{-3} . To obtain the hard mask layer, dry thermal oxidation was used to form a 20 nm thick thermal silicon oxide layer. Electron-beam lithography and reactive ion etching methods were used to define the nanowire structure on the hard mask layer. To transfer the nanowire structures into the silicon layer, tetramethylammonium hydroxide (TMAH) solution below 80 °C was chosen to etch the silicon layer. This anisotropic wet etching method could reduce the number of the defects and improve the surface quality of silicon nanowires. The boron ion implantation process was then performed on the source and drain regions followed by the rapid thermal annealing process at a temperature of 1000 °C for 5 s to produce a better quality of ohmic contact. The gate dielectric layer was then grown by means of dry thermal oxidation to a thickness of 8 nm. After the back gate was fabricated by etching through the buried oxide layer, the ohmic contact was performed by thermal evaporation of 100 nm chromium and 200 nm gold, the lift-off process, and annealing. To protect the contact pads during the measurement, the passivation layer was formed by spin coating the polyimide waterproof layer in which the liquid exposure windows over the nanowire regions were opened by lithography. Finally, after cutting the wafers into small chips, the samples were then wire-bonded, encapsulated using two glass rings as well as polydimethylsiloxane (PDMS), and ready for measurement.

The samples were placed in the custom-built Faraday cage, to protect the signal from external electromagnetic radiation. The current-voltage characteristics of nanowire sensor with $Ag/AgCl_2$ reference electrode immersed into a liquid were measured using a Keithley 2400 measurement device. For the noise measurement, the low noise measurement setup was used in the laboratory. In the low noise measurement setup, the two rechargeable batteries combined with the variable resistors were chosen as the source biases and the gate-source applied voltage to the sample. To stabilize the voltage, the capacitance was also connected to the voltage supply system. The signals from the transistor were first pre-amplified by an ultra-low internal noise preamplifier. The ITHACO 1201 amplifier was then used to further amplify the signal. Using the Agilent U2542A simultaneous data acquisition module and a high-speed USB 2.0, the signal data were transferred to the PC, where the voltage noise power spectral density (S_v) was extracted from 1 Hz to 100 kHz by a fast Fourier transform.

Statistical Analysis: Noise properties of several identical NW FET samples are investigated. Samples are fabricated using SOI wafer with 50 nm $\langle 100 \rangle$ -oriented silicon low-doped layer with doping concentration of 10^{15} cm^{-3} . A 25 nm moderately doping (10^{16} cm^{-3}) silicon layer was epitaxial overgrown on top of 50 nm silicon layer with B-dopants to obtain p-type conductivity TL channel after the processing of nanowire FETs. A 100 nm wide and 800 nm long liquid-gated TL NW FETs are studied using I - V characteristics and noise spectroscopy. Initially obtained data represent the voltage spectral density of noise, $S_v(f)$ measured as a function of frequency

$$S_v(f) = \lim_{\Delta f \rightarrow 0} \frac{\langle (V - \bar{V})^2 \rangle}{\Delta f} \quad (3)$$

where $\langle (V - \bar{V})^2 \rangle$ is the root mean square voltage fluctuation in the frequency band Δf .

The 100 noise spectra, from the same NW FET, operating in a definite regime, have been measured using a homemade measurement program using Fourier transformation of the data from time domain to frequency domain. After averaging of 100 noise spectra, one resulting spectrum is plotted and used for further analysis. The measurement error is estimated to be below 10%. The measured spectra also contains a contribution from the thermal noise of the equivalent resistance,

consisting of the resistances connected in parallel, the sample resistance, the load resistance, and the input resistance of the low-noise amplifier.

Therefore, the noise equivalent resistance $S_{V,therm}(f) = 4kTR_{eq}$ has to be subtracted from measured noise:

$$S_{V,real}(f) = S_V(f) - 4kTR_{eq} \quad (4)$$

For further calculations, it is convenient to use the spectral density of current fluctuations

$$S_I(f) = S_{V,real}(f) / R_g^2 \quad (5)$$

The noise properties of different samples measured at different voltages can be compared using the dimensionless Hooge parameter, which is characteristic of the noise level of a measured sample with respect to other samples studied in different conditions. To estimate the Hooge parameter, we used Equation (2) (see the text of the article):

$$\alpha_H(f) = \frac{S_I(f) f L^2 R}{V_D^2 q \mu_p} \quad (6)$$

This representation allows clear identification of the spectral deviations from the dependence $1/f$, which corresponds to flicker noise and represents the main component of noise spectra in metal oxygen semiconductor (MOS) FET devices. In this representation, the frequency slopes in the spectrum are reduced by 1, and the $1/f$ component of the noise spectrum is represented by a horizontal line, and the generation-recombination (GR) component can be analyzed as a bump (see, for example, Figure 6 of the article).

Since the deviations of the spectra from $1/f$ are small in many cases, smoothing of the spectral curves was applied to better analyze them. At the same time, in order to avoid the loss of information about the appearance of artifacts, it was taken into account that in the equilibrium state, the slope of the spectra cannot exceed 2 in absolute value (in this representation of the spectra, it is about 1). Smoothing was performed using the OriginPro. An example of smoothing is shown in the Figure S1, Supporting Information (see an example of the smoothing procedure):

The smoothing procedure does not distort the spectrum and satisfies the abovementioned requirements.

Supporting Information

Supporting Information is available from the Wiley Online Library or from the author.

Acknowledgements

Y.K. is very grateful for a research grant received from the German Academic Exchange Service (DAAD). Y.G. is grateful for Joint CAS-DAAD PhD Training Scholarship Program between the Chinese Academy of Sciences (CAS) and the DAAD.

Open access funding enabled and organized by Projekt DEAL.

Conflict of Interest

The authors declare no conflict of interest.

Data Availability Statement

The data that support the findings of this study are available from the corresponding author upon reasonable request.

Keywords

biosensors, Hooge parameters, noise spectra, silicon nanowire transistors, space-charge-limited current effect

Received: May 23, 2022

Revised: August 8, 2022

Published online: October 10, 2022

- [1] a) P. Bergveld, *IEEE Trans. Biomed. Eng.* **1972**, 19, 342; b) F. Patolsky, G. Zheng, O. Hayden, M. Lakadamyali, X. Zhuang, C. M. Lieber, *Proc. Natl. Acad. Sci. USA* **2004**, 101, 14017; c) F. Patolsky, G. Zheng, C. M. Lieber, *Nat. Protoc.* **2006**, 1, 1711; d) K.-I. Chen, B.-R. Li, Y.-T. Chen, *Nano Today* **2011**, 6, 131; e) Y. Cui, Q. Wei, H. Park, C. M. Lieber, *Science* **2001**, 293, 1289; f) J. Li, Y. Kutovyi, I. Zadorozhnyi, N. Boichuk, S. Vitusevich, *Adv. Mater. Interfaces* **2020**, 7, 2000508; g) S. Vitusevich, I. Zadorozhnyi, *Semicond. Sci. Technol.* **2017**, 32, 043002; h) K. Zekentes, J. Choi, V. Stambouli, E. Bano, O. Karker, K. Rogdakis, *Microelectron. Eng.* **2022**, 255, 111704.
- [2] a) J. Li, S. Pud, M. Petrychuk, A. Offenhäusser, S. Vitusevich, *Nano Lett.* **2014**, 14, 3504; b) Y. Kutovyi, V. Piatnytsia, N. Boichuk, I. Zadorozhnyi, J. Li, M. Petrychuk, S. Vitusevich, *Adv. Electron. Mater.* **2021**, 7, 2000858; c) Y. Kutovyi, I. Zadorozhnyi, V. Handziuk, H. Hlukhova, N. Boichuk, M. Petrychuk, S. Vitusevich, *Nano Lett.* **2018**, 18, 7305; d) Y. Kutovyi, H. Hlukhova, N. Boichuk, M. Menger, A. Offenhäusser, S. Vitusevich, *Biosens. Bioelectron.* **2020**, 154, 112053.
- [3] S. X. Li, W. Guan, B. Weiner, M. A. Reed, *Nano Lett.* **2015**, 15, 5046.
- [4] a) B. I. Shklovskii, *Phys. Rev. E* **1999**, 60, 5802; b) E. Wernersson, R. Kjellander, J. Lyklema, *J. Phys. Chem. C* **2010**, 114, 1849.
- [5] D. E. Yates, S. Levine, T. W. Healy, *J. Chem. Soc., Faraday Trans. 1* **1974**, 70, 1807.
- [6] A. Tarasov, M. Wipf, R. L. Stoop, K. Bedner, W. Fu, V. A. Guzenko, O. Knopfmacher, M. Calame, C. Schönenberger, *ACS Nano* **2012**, 6, 9291.
- [7] D. Sobczyńska, W. Torbicz, *Sens. Actuators* **1984**, 6, 93.
- [8] M. Wipf, R. L. Stoop, A. Tarasov, K. Bedner, W. Fu, I. A. Wright, C. J. Martin, E. C. Constable, M. Calame, C. Schönenberger, *ACS Nano* **2013**, 7, 5978.
- [9] R. Sivakumarasamy, R. Hartkamp, B. Siboulet, J.-F. Dufrêche, K. Nishiguchi, A. Fujiwara, N. Clément, *Nat. Mater.* **2018**, 17, 464.
- [10] K. B. Parizi, X. Xu, A. Pal, X. Hu, H. Wong, *Sci. Rep.* **2017**, 7, 41305.
- [11] A. Many, S. Weisz, M. Simhony, *Phys. Rev.* **1962**, 126, 1989.
- [12] a) A. A. Talin, F. Léonard, B. Swartzentruber, X. Wang, S. D. Hersee, *Phys. Rev. Lett.* **2008**, 101, 076802; b) A. A. Talin, F. Léonard, A. Katzenmeyer, B. Swartzentruber, S. Picraux, M. Toimil-Molares, J. Cederberg, X. Wang, S. Hersee, A. Rishinaramangalum, *Semicond. Sci. Technol.* **2010**, 25, 024015; c) Y. Gu, L. Lauhon, *Appl. Phys. Lett.* **2006**, 89, 143102; d) A. D. Schrick, F. M. Davidson, R. J. Wiacek, B. A. Korgel, *Nanotechnology* **2006**, 17, 2681; e) Z.-M. Liao, Z.-K. Lv, Y.-B. Zhou, J. Xu, J.-M. Zhang, D.-P. Yu, *Nanotechnology* **2008**, 19, 335204; f) P. Zhang, Y. S. Ang, A. L. Garner, Á. Valfells, J. Luginsland, L. Ang, *J. Appl. Phys.* **2021**, 129, 100902; g) S. Alagha, A. Shik, H. E. Ruda, I. Saveliev, K. L. Kavanagh, S. P. Watkins, *J. Appl. Phys.* **2017**, 121, 174301.
- [13] a) R. Yamanaka, Y. Shindo, K. Oka, *Int. J. Mol. Sci.* **2019**, 20, 3439; b) Y. Hu, Z. Chen, Z. Hou, M. Li, B. Ma, X. Luo, X. Xue, *Molecules* **2019**, 24, 2091.
- [14] A. Zulfikar, F. Patou, A. Pfreundt, C. Papakonstantinou, W. E. Svendsen, M. Dimaki, *Sens. Biosens. Res.* **2017**, 13, 88.
- [15] a) V. Sydoruk, I. Zadorozhnyi, H. Hardtdegen, H. Lüth, M. Petrychuk, A. Naumov, V. Korotkyev, V. Kochelap, A. Belyaev,

- S. Vitusevich, *Nanotechnology* **2017**, *28*, 135204; b) V. Sydoruk, S. Vitusevich, H. Hardtdegen, M. Petrychuk, A. Naumov, V. Korotyeyev, V. Kochelap, A. Belyaev, *Fluctuation Noise Lett.* **2017**, *16*, 1750010.
- [16] N. F. Mott, R. W. Gurney, *Electronic Processes in Ionic Crystals*, Clarendon Press, Oxford **1948**.
- [17] Y. Kutovyi, I. Zadorozhnyi, H. Hlukhova, V. Handziuk, M. Petrychuk, A. Ivanchuk, S. Vitusevich, *Nanotechnology* **2018**, *29*, 175202.
- [18] B. Shougaijam, R. Swain, C. Ngangbam, T. Lenka, *J. Semicond.* **2017**, *38*, 053001.
- [19] N. B. Lukyanchikova, B. Jones, *Noise Research in Semiconductor Physics*, CRC Press, Boca Raton, FL **2020**.
- [20] S. A. Vitusevich, S. V. Danylyuk, N. Klein, M. V. Petrychuk, V. N. Sokolov, V. A. Kochelap, A. E. Belyaev, V. Tilak, J. Smart, A. Vertiatchikh, L. F. Eastman, *Appl. Phys. Lett.* **2002**, *80*, 2126.
- [21] a) F. Léonard, J. Tersoff, *Phys. Rev. Lett.* **1999**, *83*, 5174; b) M. A. Lampert, P. Mark, *Current Injection in Solids*, Academic Press, New York, USA **1970**; c) A. A. Grinberg, S. Luryi, M. Pinto, N. Schryer, *IEEE Trans. Electron Devices* **1989**, *36*, 1162.